Supramolecular polymers with tunable topologies via hierarchical coordination-driven self-assembly and hydrogen bonding interfaces

Xuzhou Yan[a,b], Shijun Li[b,c], James Bryant Pollock[b], Timothy R. Cook[b], Jianzhuang Chen[a], Yanyan Zhang[d], Xiaofan Ji[a], Yihua Yu[d], Feihe Huang[a,1], and Peter J. Stang[b,1]

[a]Ministry of Education Key Laboratory of Macromolecular Synthesis and Functionalization, Department of Chemistry, Zhejiang University, Hangzhou 310027, China; [b]Department of Chemistry, University of Utah, Salt Lake City, UT 84112; [c]College of Materials, Chemistry and Chemical Engineering, Department of Chemistry, Hangzhou Normal University, Hangzhou 310036, China; and [d]Shanghai Key Laboratory of Magnetic Resonance, Department of Physics, East China Normal University, Shanghai 200062, China

Contributed by Peter J. Stang, April 19, 2013 (sent for review March 28, 2013)

A powerful strategy to obtain complex supramolecular materials is the bottom-up construction of noncovalently bound materials by hierarchical self-assembly. This assembly process involves stepwise, uniform increases to the architectural complexity of a substrate, starting from discrete precursors and growing in dimensionality through controlled reactivity to a final product. Herein, two orthogonal processes are exploited: coordination-driven self-assembly and hydrogen bonding. The former relies on the predictable formation of metal–ligand bonds wherein the directionalities of the rigid precursors used determines the structural outcome. The latter uses 2-ureido-4-pyrimidinone interfaces that are structurally robust by virtue of the quadruple hydrogen bonding that can occur between subunits. By combining these two processes into a single system, it is possible to generate hierarchical materials that preserve the attractive tunability associated with discrete supramolecular coordination complexes. For instance, the synthesis of a one-dimensional chain comprising linked metalla-rhomboids is readily adapted to a 2D cross-linked hexagonal network by simply selecting a different metal acceptor precursor as an assembly component. The specific interactions between subunits, in this case platinum(II)-pyridyl bonds and the quadruple H-bonding of ureidopyrimidinone, are unchanged, establishing a unique strategy to obtain supramolecular polymers with marked topological differences with minimal synthetic redesign. In addition, the structural rigidity imposed by the inclusion of the platinum metallacycles serves to minimize the formation of cyclic oligomers, increasing the efficacy of formation and improving the properties of the resultant materials. Furthermore, this study taps the potential of organoplatinum(II) metallacycles in materials science.

Nature provides many examples of structurally complex and functional architectures by integrating multiple simple interactions that act in concert to produce the final macro- or supramolecular compound. For example, the primary structure of a protein comprises covalent amide bonds. Secondary structure is concerned with the formation of local segments of peptide chains as defined by simple hydrogen bonding. The next level of complexity, tertiary structure, is largely determined by hydrophobic interactions with contributions from disulfide bonds. Taken separately, these interactions are basic and fundamental in chemistry, yet when combined as components of hierarchical synthesis, impressive examples of complex, functional proteins may be found (1). Natural systems remain an ongoing motivation for scientists seeking new methods to obtain elaborate molecular assemblies using simple interactions as the impetus for formation. Hierarchical polymerization, in which growing complexity is achieved through well-defined steps that iteratively increase the dimensionality of a material, is particularly attractive in that each unique interaction can be carefully designed. As with proteins, the local interactions between the smallest subunits are often simple, yet taken as a whole, these interactions lead to complex architectures over various length scales (2, 3). In some cases, the most effective means to emulate natural systems is simply to exploit the moieties found therein. As such, the nucleobases found in DNA have been incorporated into numerous polymerization strategies that take advantage of their proclivity to hydrogen bond and provide favorable electrostatic interactions (4). Related examples can be found in the form of peptide amphiphiles that, on self-assembly and mineralization, can form nanofibers (5), as well as abiological organic polymers that form helical rods that exhibit host–guest chemistry (6), all with relatively simple interactions as their impetus for formation.

Organizing a single type of interaction between subunits is itself useful, and as new methods for controlling H-bonding, hydrophobic interactions, π-π stacking, Van de Waals forces, and metal-ligand bonding emerge, impressive examples of novel supramolecular polymeric materials tend to follow (7). For instance, organic precursors with hydrogen bonding interfaces can self-assemble into columnar structures (8), a pioneering example in a field that has steadily grown to include a number of materials (9–16), which have helped establish supramolecular polymerization as a critical subset of materials science (7, 17–20).

Metal–ligand bonding has proven to be a particularly valuable method to guide the organization of molecular precursors through strategies such as coordination-driven self-assembly (21–26). By carefully combining selected building blocks, discrete supramolecular coordination complexes (SCCs) can be obtained (27–31), based on the number and orientation of the labile coordination sites (for metal acceptors) and Lewis basic moieties (for organic donors). Because these metal–ligand interactions are general for a wide number of transition metals and organic linkers, a sizable library of 2D and 3D structures spanning multiple synthetic approaches has been developed over the last two decades. These synthetic strategies are unified under the theme of directional bonding, which reduces a target architecture to its constituent edges, faces, and vertices and seeks to replicate these on a molecular level (27). The substantial body of synthetic research has paved the way for multifunctional applications of SCCs ranging from molecular topology (32–34) and catalysis (35, 36) to light harvesting and gas capture (37, 38).

Herein, we unify the themes of coordination-driven self-assembly and supramolecular polymerization through a hierarchical design strategy. Two SCC platforms are used, a [2 + 2] rhomboid constructed from a 60° acceptor and a 120° donor and hexagonal

Author contributions: X.Y., F.H., and P.J.S. designed research; X.Y., S.L., J.B.P., J.C., Y.Z., X.J., and Y.Y. performed research; X.Y. contributed new reagents/analytic tools; X.Y. and S.L. analyzed data; and X.Y., T.R.C., F.H., and P.J.S. wrote the paper.

The authors declare no conflict of interest.

[1]To whom correspondence may be addressed. E-mail: fhuang@zju.edu.cn or stang@chem.utah.edu.

This article contains supporting information online at www.pnas.org/lookup/suppl/doi:10.1073/pnas.1307472110/-/DCSupplemental.

metallacycles that result from the [3 + 3] assembly of 120° acceptors and the same 120° donor. The self-assembly that occurs spontaneously on mixing these building blocks represents one component of the polymerization. To link these discrete metallacycles together, a second orthogonal interaction was designed to take advantage of hydrogen bonding. Specifically, the well-defined quadruple hydrogen bonding motif, 2-ureido-4-pyrimidinone (UPy), as developed by Meijer and coworkers, was selected (39). The UPy motif complements coordination-driven self-assembly by offering an attractive combination of high thermodynamic stability (ΔG = ~10 Kcal/mol; $k_{dimer} > 10^7$ M^{-1} in chloroform) and rapid kinetic reversibility (k_{off} = ~8 s^{-1}) (39). These favorable parameters have been previously exploited to link UPy-containing subunits, furnishing supramolecular polymers with high synthetic efficiencies and possessing dynamic reversibility (10, 17, 40). Moreover, the presence of self-selective UPy moieties was not expected to disrupt the platinum (Pt)–pyridyl bonding used for metallacycle formation, meaning the two interactions could independently occur within a single reaction flask. Coordination-driven self-assembly of the UPy-functionalized ligand with metal acceptors resulted in metallacycles decorated with a number of pendant hydrogen bonding sites. Hydrogen bonding could be mediated by selecting an appropriate solvent, thus linking the metallacycles into supramolecular polymers. This work establishes (1) the UPy functionalization of a 120° dipyridyl ligand through aryl-ether and amide linkers, which is readily used in (2) the formation of bis (phosphine) Pt(II) rhomboidal and hexagonal metallacycles decorated with H-bonding moieties that facilitate (3) the formation of linear chains (rhomboid) or cross-linked supramolecular polymers (hexagons; Fig. 1). The resulting materials highlight the advantages of SCC-based supramolecular polymers, in particular by attenuating the formation of cyclic oligomers due to the rigidity of the metallacyclic subunits. These polymers exhibit solvent swelling effects and the adaptive deformation of the cross-linked hexagonal networks via external forces results in macroscopic fibers that are robust enough to arrange into a knot. The strength, stretchability, and flexibility of these fibers is attributed to the ability of the cross-linked hexagons to reestablish Pt-pyridyl bonds that may be severed on mechanical stress, a property that is absent in supramolecular polymers that lack the SCC component described here.

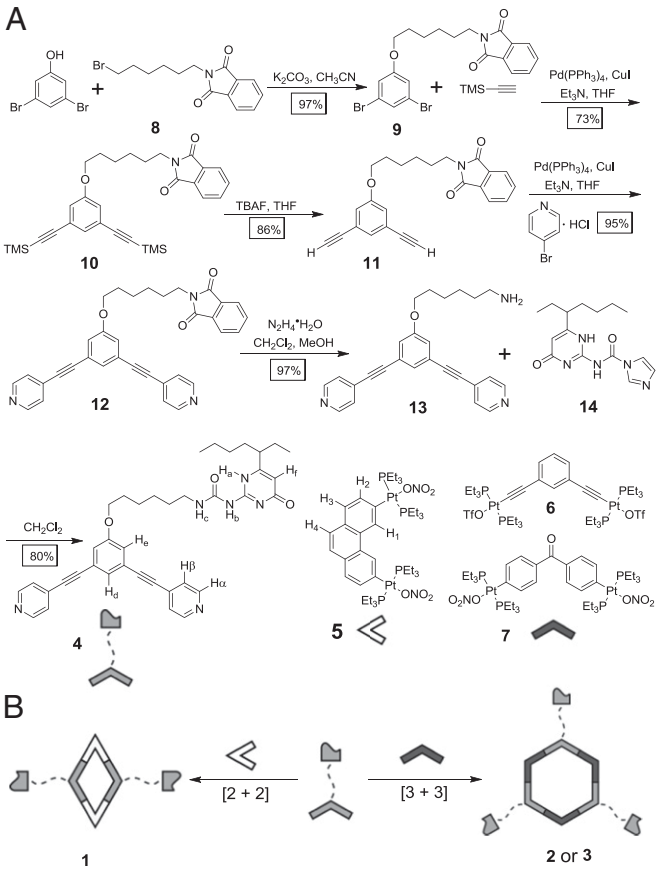

Scheme 1. Preparation of metallasupramolecules **1**–**3**. (*A*) Synthetic route for the UPy-functionalized 120° dipyridyl donor **4**. (*B*) Cartoon representation of the formations of UPy-functionalized rhomboid **1** and hexagons **2** and **3**.

Results and Discussion

The UPy-functionalized 120° dipyridyl donor (**4**) was synthesized in a six-step pathway starting from commercially available 3,5-dibromophenol (Scheme 1*A*). After nucleophilic substitution of the phenolic hydroxyl, palladium-catalyzed introduction of the TMS-protected acetylene (**10**, 73% isolated yield) and subsequent desilylation in 86% isolated yield, compound **11** was reacted with 4-bromopyridine hydrochloride via a Sonogashira coupling to give 120° dipyridyl ligand **12** in 95% isolated yield. This stable isoindoline-1,3-dione precursor is particularly useful in that it can be readily reduced to amino intermediate **13** in the presence of hydrazine (97% isolated yield). Given the well-established coupling reactions of primary amines, this compound provides a generalized route to furnish 120° donors functionalized with any moiety that is compatible with amine couplings. Herein, we linked amine-terminated compound **13** with a 1,1′-carbonyldiimidazole-activated alkyl-substituted pyrimidinone (**14**), delivering the 120° UPy-functionalized dipyridyl ligand (**4**) with an 80% isolated yield.

Stirring a mixture of **4** and 60° organoplatinum(II) acceptor 3,6-bis[*trans*-$Pt(PEt_3)_2(NO_3)_2$]phenanthrene (**5**) in a 1:1 ratio in CD_3OD at 50 °C for 8 h induced the self-assembly of [2 + 2] rhomboid **1** decorated with UPy at its vertices (Scheme 1*B*). Self-assembled [3 + 3] hexagons were prepared in a similar fashion by mixing **4** with one of two 120° organoplatinum(II) acceptors, 1,3-bis[*trans*-$Pt(PEt_3)_2(OTf)_2$ ethynyl]benzene (**6**; forming hexagon **2**) or 4,4′-[*trans*-$Pt(PEt_3)_2(NO_3)_2$]diphenyl ketone (**7**; forming hexagon **3**), in a 1:1 ratio in DMSO-d_6 at 50 °C for 8 h (Scheme 1*B*). Multinuclear NMR (^1H and ^{31}P) analyses of the reaction mixtures supported the formation of discrete, highly symmetric species (Fig. 2; *SI Appendix*). The ^{31}P $\{^1H\}$ NMR spectrum of hexagon **2**, for example, revealed a sharp singlet at ~13.15 ppm with concomitant ^{195}Pt satellites ($J_{Pt\text{-}P}$ = 2,309.5 Hz), consistent with a single phosphorous environment (Fig. 2, spectrum *D*). This peak was shifted upfield relative to that of acceptor **6** by ~5.97 ppm (*SI Appendix*, Fig. S23*B*). The spectra of **1** and **3** similarly possessed single sharp peaks with Pt satellites (Fig. 2; *SI Appendix*).

Electrospray ionization time of flight mass spectrometry provided further evidence for the formations of discrete UPy-functionalized rhomboid **1** and hexagons **2** and **3**. In the mass spectrum of **1**, five peaks were observed that supported a [2 + 2] structural assignment (*SI Appendix*, Fig. S21) including those that corresponded to an intact assembly with charge states resulting from the loss of nitrate counterions ($[M - 2NO_3]^{2+}$ m/z = 1,731.71; $[M - 3NO_3]^{3+}$ m/z = 1,133.79; *SI Appendix*, Fig. S21). For hexagon **2**, eight peaks were found (*SI Appendix*, Fig. S24). The peak at m/z = 1,000.40 is consistent with an intact $[M - 5OTf]^{5+}$ charge state, expected only for a [3 + 3] assembly. Similarly, eight peaks were found for hexagon **3** (*SI Appendix*, Fig. S27), including that which corresponded to the intact $[M - 5NO_3]^{5+}$ charge state at m/z = 1,016.43. All of these peaks were isotopically resolved and agreed very well with their calculated theoretical distributions. Given the difficulty associated with obtaining single crystals suitable for X-ray diffraction for molecules containing long alkyl spacers, crystallographic studies were elusive. However, the structural characteristics of **1**–**3** were simulated via molecular mechanics universal force-field (UFF) calculations (*SI Appendix*, Fig. S28). The theoretical structures share common characteristics including planar metallacyclic cores with exohedral functionalization by the pendant UPy motifs, which

extend above and below the cores (*SI Appendix*, Fig. S28). As such, these UPy groups are well situated to undergo intermolecular hydrogen bonding.

In the ^{1}H NMR spectrum of rhomboid **1**, downfield shifts of the α- and β-pyridyl protons relative to those of ligand **4** were observed, consistent with the loss of electron density that occurs on Pt–pyridyl bond formation. As shown in Fig. 3 (spectrum *H*), the α- and β-pyridyl protons are split into two sets of two doublets on coordination. The H_α protons (8.62 ppm in **4**; Fig. 3, spectrum *I*) are split into two doublets at 9.31 and 8.74 ppm (Fig. 3, spectrum *H*). Similarly, the H_β protons (7.41 ppm in **4**; Fig. 3, spectrum *I*) are also split into two doublets, at 7.94 and 7.81 ppm (Fig. 3, spectrum *H*).

The orthogonal relationship between the metal–ligand bonding responsible for SCC formation and the H-bonding expected of the UPy moieties manifests in two routes toward polymer formation. If a solvent such as methanol or DMSO is used, SCC formation occurs under conditions in which UPy dimerization is blocked due to hydrogen bonding with solvent molecules. The discrete metallacycles thus formed can then be polymerized by dissolution in a solvent that facilitates UPy–UPy interactions, such as CH_2Cl_2. Alternatively, the dissolution of **4** in CH_2Cl_2 will result in the formation of dimeric ligands that will self-assemble into polymeric materials directly on the introduction of metal acceptor **5** (*SI Appendix*, Fig. S29).

The formation of linear chains of **1** (Fig. 1*A*) was indicated by ^{1}H NMR spectra in CD_2Cl_2 at concentrations ranging from 1.00 to 110 mM (Fig. 3, spectra *A*–*H*). The UPy N–H signals displayed large downfield shifts (observed between 10.0 and 13.5 ppm) and a lower intensity relative to the one in DMSO, giving direct evidence for the formation of H-bonds between UPy groups. Furthermore, the chemical shifts of the UPy protons showed little change on increasing monomer concentration. The single set of signals of the UPy protons indicates that there is no significant formation of low-molecular-weight cyclic oligomers. The lack of cyclic oligomers was also supported by 2D diffusion-ordered ^{1}H NMR spectroscopy (DOSY) NMR (*vide infra*). The circumvention of oligomer formation is attributed to the rigidity of the metallacyclic cores, which limits the formation of cyclic species and thereby improves the efficiency of polymerization in SCC–UPy systems. As the concentration of **1** approaches 40.0 mM, the H_1 signal associated with acceptor **5** shifts upfield, ultimately overlapping with one set of the H_α protons resonances (Fig. 3, spectrum *D*). Above 20.0 mM, the peaks undergo broadening that obscures the well-resolved splitting associated with the free ligand and indicates the formation of high-molecular-weight rhombic aggregates (14, 19). Despite these spectral changes in the ^{1}H NMR, the ^{31}P {^{1}H} NMR spectra of **1** have no significant concentration dependencies, with the exception of some broadening that occurs at high concentrations (*SI Appendix*, Fig. S30).

DOSY was used to probe the dimensions of the polydispersed supramolecular aggregates (14, 19). As the concentration of rhomboid **1** was increased between 10.0 and 90.0 mM, the measured weight average diffusion coefficient decreased from 1.07×10^{-10} to 5.83×10^{-12} $m^2 \cdot s^{-1}$ ($D_{10.0\ mM}/D_{90.0\ mM} \sim 19$; Fig. 4*A*, *b*–*g*), indicating a concentration dependence on the polymerization of **1** to give high-molecular-weight structures. On the DOSY NMR time scale, no evidence for low-molecular-weight cyclic oligomer formation was observed (*SI Appendix*, Figs. S32–S37), further supporting the utility of rigid metallacyclic cores in producing high fidelity polymers. The supramolecular entities have narrow dispersities at the concentration ranges of **1** used here. The DOSY NMR of unfunctionalized rhomboid **15** was also performed using a 20.0-mM solution to yield an average diffusion coefficient of 3.94×10^{-10} $m^2 \cdot s^{-1}$ (Fig. 4*A*, *a*; *SI Appendix*, Fig. S31), further supporting that the UPy moieties are responsible for aggregate formation in CD_2Cl_2. Moreover, dynamic light scattering (DLS) measurements were conducted to

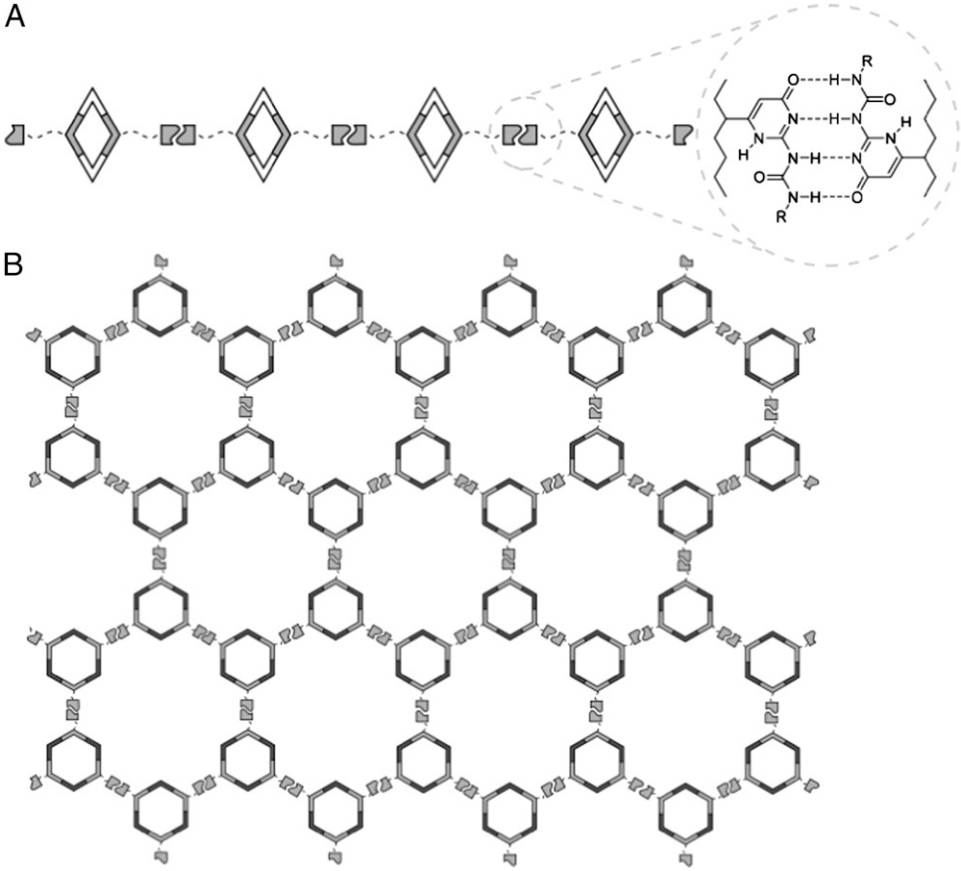

Fig. 1. Cartoon representations for the formation of a linear supramolecular polyrhomboid (*A*) and cross-linked three-dimensional supramolecular polymeric networks (*B*) from self-assembly of rhomboid **1** and hexagon **2** or **3**, respectively.

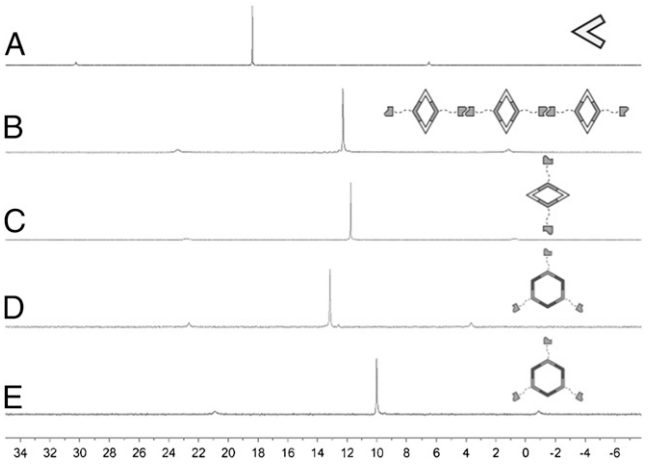

Fig. 2. ^{31}P {^{1}H} NMR spectra (room temperature, 121.4 MHz) of (*A*) 60° acceptor **5** in CD_2Cl_2, (*B*) supramolecular polyrhomboid in CD_2Cl_2 at a concentration of 40.0 mM **1**, (*C*) rhomboid **1** in CD_3OD, (*D*) hexagon **2** in DMSO-d_6, and (*E*) hexagon **3** in DMSO-d_6.

study the size distributions of the polymeric material with respect to the concentration of **1** (Fig. 4*B*). At the concentration of 10.0 mM, polymerized **1** showed an average hydrodynamic diameter (D_h) value of 205.2 nm. The value of D_h was concentration dependent, increasing at higher molarities, indicating that larger aggregates are formed when more **1** is present. Given the ∼5-nm size of rhomboid **1** as predicted by the force-field calculations, the measured average D_h obtained by DLS suggest that there are ∼41 rhombic units in the linear polymeric chain at 10.0 mM.

Although the polymeric material comprised of rhomboid **1** was sufficiently soluble to allow for the solution-based characterization methods described above, rod-like fibers could be mechanically drawn from high viscosity CH_2Cl_2 solutions. These fibers were imaged using SEM (*SI Appendix*, Fig. S44), providing evidence for the formation of a polymeric material formed via linkage of the rhomboids into a linear chain. Furthermore, transmission electron microscopy (TEM) was used to provide further insight into the hierarchical assembly of the polymer material. As shown in Fig. 5*C*, samples of **1** ultimately organize into long fibers with a diameter of ∼300 nm. These fibers represent bundles of single strands of linear rhomboid chains that rapidly form in solution as the UPy moieties undergo hydrogen bonding. Once formed, these single polymeric chains aggregate in solution, entangling together to form associated clusters which ultimately self-assemble into tightly packed nanoscale fibers (Fig. 5*A*).

Subsequently, we used UPy-functionalized hexagons **2** and **3** to prepare cross-linked supramolecular hexagonal networks (Fig. 1*B*) with the aim of exploiting their material properties benefiting from the introduction of organoplatinum(II) metallacycles. However, solution-based characterization techniques could not be used to investigate the polymerization of UPy-functionalized hexagons **2** and **3** due to the insoluble materials that formed on introduction of solvents that facilitated hydrogen bonding. The anticipated cross-linked polymer networks (Fig. 1*B*) expected for these hexagonal metallacycles could instead be studied by FTIR methods, which indicated bands associated with N–H hydrogen bond formation and characteristic signatures of the ethynyl moieties of ligand **4** (*SI Appendix*, Figs. S39–S41). Despite the lack of solubility of polymeric **2** and **3** in dichloromethane, the introduction of this solvent resulted in the formation of gel-like soft matter due to swelling (Fig. 5*B*). The swelling properties of cross-linked polymeric materials are well established, and the observation of such a phenomenon with **2** and **3** supported the formation of extended hexagonal networks. Swelling tests based on the sample weight before and after swelling indicated that the network resulting from **3** exhibited a larger effect than that of hexagon **2** (*SI Appendix*, Figs. S42 and S43). Attempts to draw out macroscopic fibers from the swelled samples resulted in the formation of long, flexible fibers (Movie S1). SEM imaging established that fibers obtained from gels of **2** had diameters of ∼8 μm (Fig. 5*D*). As a testament to the stretchability, flexibility, and strength of the resulting material, one such fiber, obtained from a gel of **3**, was readily fashioned into an overhand knot. The knot structure persisted over the course of 24 h, with no cracking or agglomeration. The combination of stretchability, strength, and flexibility associated with the formation of such a structure deriving from multicomponent self-assembly based on low-molecular-weight building blocks is noteworthy and illustrates the promising characteristics of SCC-based supramolecular polymers, which are reminiscent of the skeletal muscle protein titin, which possesses a remarkable combination of strength, toughness, and elasticity (41). The observed properties of the cross-linked hexagonal networks are attributed in part to the efficient polymerization that can occur when rigid metallacyclic cores are present. These cores preorient their pendant UPy groups for the facile formation of hexagonal networks. On mechanical stress, which can potentially rupture both H-bonding and the SCC cores, both the metal–ligand coordination and UPy dimerization can readily reform due to the reversibility of both processes. These features allow the material to adapt to physical deformations by stabilizing new orientations of the precursors through intermolecular bond formation, ultimately increasing the robustness of the materials. Even if mechanical stress distorts the cores such that hexagons cannot reform, the multitopic nature of the precursors ensures that some cross-linking can persist, thereby increasing the cross-link density and strengthening the new 3D network.

Conclusion

In summary, by combining the directional-bonding approach of coordination-driven self-assembly and the quadruple hydrogen bonding of UPy moieties, we established a method for hierarchical supramolecular polymerization. The tunability associated with SCC formation allowed for the formation of both a rhomboid and two hexagons from a single UPy-functionalized dipyridyl ligand by selecting specific metal acceptors. The hierarchical supramolecular polymerization of this ligand furnished discrete SCCs decorated with UPy groups as a first level of complexity. The complexity was then amplified on hydrogen bonding of the UPy groups to link the metallacycles into either a linear chain (rhomboid) or cross-linked networks (hexagons). Characterization

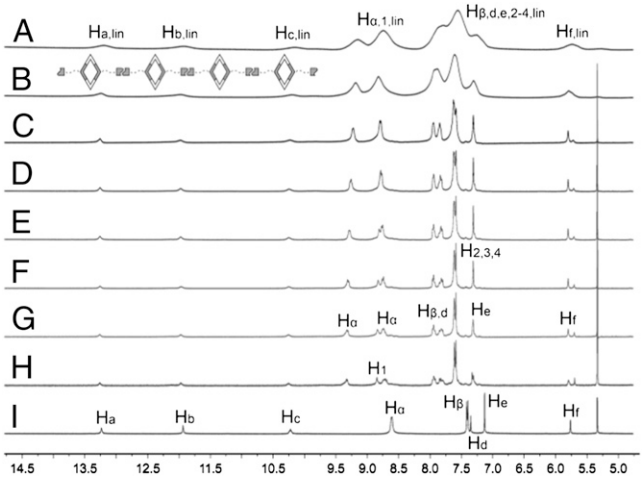

Fig. 3. Partial ^{1}H NMR spectra of rhomboid **1** (CD_2Cl_2, room temperature, 300 MHz) at different concentrations: (*A*) 110 mM; (*B*) 78.0 mM; (*C*) 60.0 mM; (*D*) 40.0 mM; (*E*) 20.0 mM; (*F*) 10.0 mM; (*G*) 5.00 mM; (*H*) 1.00 mM; and (*I*) 120° UPy-functionalized ligand **4** in CD_2Cl_2. Peaks of linear polymer are designated by lin.

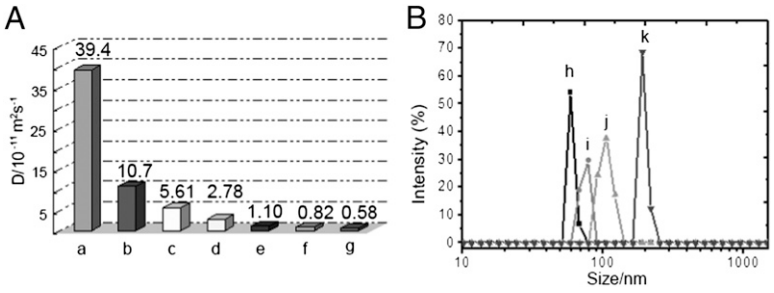

Fig. 4. Solution-state size analyses of supramolecular polyrhomboid. (*A*) The measured weight average diffusion coefficient *D* (CD_2Cl_2, room temperature, 500 MHz): a, parent rhomboid **15** at 20.0 mM, and rhomboid **1** at (*b*) 10.0 mM; (*c*) 20.0 mM; (*d*) 40.0 mM; (*e*) 65.0 mM; (*f*) 75.0 mM; (*g*) 90.0 mM. (*B*) Size distributions of UPy-functionalized rhomboid **1** at different concentrations: (*h*) 1.25 mM, D_h = 63.4 nm; (*i*) 2.50 mM, D_h = 73.4 nm; (*j*) 5.00 mM, D_h = 106.5 nm; (*k*) 10.0 mM, D_h = 205.2 nm.

of the resulting materials revealed that the polymerizations were particularly effective in avoiding the formation of low-molecular-weight cyclic oligomers, a property attributed to the presence of the rigid metallacyclic cores. In addition, the solvent swelling formation of gels observed for the hexagonal networks lent themselves to the formation of long, macroscopic fibers that possessed enough strength and flexibility to permit the construction of stable knots. The robustness of these fibers is consistent with heightened cross-link densities that occur due to the reversibility of the metal–ligand and hydrogen bonding that form the material. Deformations that can permanently sever polymer strands in other materials can reform in these gel-like soft matters, restoring intermolecular cross-linking and allowing the fibers to adapt to stresses. Given the vast library of readily functionalized SCCs and favorable properties of supramolecular polymers established here, the hierarchical polymerization of metallacycles is a promising new method to obtain novel functional materials.

Materials and Methods

All reagents were commercially available and used as supplied without further purification. Deuterated solvents were purchased from Cambridge Isotope Laboratory. Compounds **5** (42), **6** (32), **7** (32), **8** (43), **14** (39), and parent rhomboid **15** (44) were prepared according to published procedures. NMR spectra were recorded on a Varian Unity 300 MHz spectrometer. ^{1}H and ^{13}C NMR chemical shifts are reported relative to residual solvent signals, and ^{31}P {^{1}H} NMR chemical shifts are referenced to an external unlocked sample of 85% H_3PO_4 (δ 0.0). The 2D diffusion-ordered (2D DOSY) NMR spectra were recorded on a Bruker DRX500 spectrometer. DLS was carried out on a Malvern Nanosizer S instrument at room temperature. FTIR spectra were recorded on a NEXUS 47 FTIR spectrometer. SEM investigations were carried out on a JEOL 6390LV instrument. TEM images were obtained using a Philips TECNAI-12 instrument with an accelerating voltage of 120 kV. Mass spectra were recorded on a Micromass Quattro II triple-quadrupole mass spectrometer using electrospray ionization with a MassLynx operating system. The melting points were collected on a SHPSIC WRS-2 automatic melting point apparatus.

In a 1:1 stoichiometric fashion, 60° or 120° bis(phosphine) organoplatinum (II) acceptor **5**, **6**, or **7** was added to the ligand **4** in a 2-dram vial. The solids were dissolved in methanol (for **1**) or DMSO (for **2** and **3**) and allowed to stir at 50 °C for 8 h. To the resulting homogeneous solution, diethyl ether was added to precipitate the product, which was then isolated and dried under reduced pressure for 4 h and redissolved in methanol or DMSO for characterization.

Rhomboid 1. ^{1}H NMR (CD_3OD, room temperature, 300 MHz) δ (ppm): 9.02 (d, J = 5.7 Hz, 4H), 8.93 (d, J = 6.0 Hz, 4H), 8.67 (s, 4H), 7.94–8.00 (m, 4H), 7.84–9.00 (m, 4H), 7.70 (s, 4H), 7.65 (s, 2H), 7.62–7.64 (m, 4H), 7.58–7.61 (m, 4H), 7.35 (d, J = 1.2 Hz, 4H), 5.85 (s, 2H), 4.12 (t, J = 6.3 Hz, 4H), 2.26–2.42 (m, 2H), 1.80–1.96 (m, 4H), 1.53–1.73 (m, 32H), 1.35–1.52 (m, 48H), 1.10–1.30 (m, 72H), 0.76–0.93 (m, 12H). ^{31}P {^{1}H} NMR (CD_3OD, room temperature, 121.4 MHz) δ (ppm): 11.76 ppm (s, ^{195}Pt satellites, $^1J_{Pt-P}$ = 2,676.4 Hz). ESI-TOF-MS: *m/z* 834.85 $[M - 4NO_3]^{4+}$, 1,112.81 $[M - HNO_3 - 3NO_3]^{3+}$, 1,124.79 $[M - 2HNO_3 - 2NO_3 + K]^{3+}$, 1,133.80 $[M - 3NO_3]^{3+}$, 1,731.68 $[M - 2NO_3]^{2+}$.

Hexagon 2. ^{1}H NMR (DMSO-d_6, room temperature, 300 MHz) δ (ppm): 11.41 (s, 3H), 9.55 (s, 3H), 8.85 (d, J = 5.7 Hz, 12H), 7.81 (d, J = 5.4 Hz, 12H), 7.54 (s, 3H), 7.52 (s, 3H), 7.39 (d, J = 5.1 Hz, 6H), 6.97–7.12 (m, 12H), 5.71 (s, 3H), 3.97–4.14 (m, 6H), 3.09–3.19 (m, 6H), 1.65–1.90 (m, 72H), 1.29–1.56 (m, 51H), 0.95–1.18 (m, 108H), 0.67–0.85 (m, 18H). ^{31}P {^{1}H} NMR (DMSO-d_6, room temperature, 121.4 MHz) δ (ppm): 13.15 ppm (s, ^{195}Pt satellites, $^1J_{Pt-P}$ = 2,309.5 Hz). ESI-TOF-MS: *m/z* 808.84 $[M - 6OTf]^{6+}$, 818.34 $[M - 2HOTf - 4OTf + Na + K]^{6+}$, 970.41 $[M - HOTf - 5OTf]^{5+}$, 977.60 $[M - 3HOTf - 3OTf + 2NH_4]^{5+}$, 1,000.40 $[M - 5OTf]^{5+}$, 1,212.50 $[M - 2HOTf - 4OTf]^{4+}$, 1,288.23 $[M - 4OTf]^{4+}$, 1,628.65 $[M - 4HOTf - 2OTf + K]^{3+}$.

Hexagon 3. ^{1}H NMR (DMSO-d_6, room temperature, 300 MHz) δ (ppm): 11.40 (s, 3H), 9.55 (s, 3H), 8.85 (d, J = 5.7 Hz, 12H), 7.84 (d, J = 5.4 Hz, 12H), 7.49–7.59 (m, 18H), 7.36–7.48 (m, 18H), 5.70 (s, 3H), 3.97–4.14 (m, 6H), 3.09–3.19 (m, 6H), 1.64–1.81 (m, 6H), 1.39–1.56 (m, 45H), 1.21–1.38 (m, 72H), 0.94–1.13 (m,108H), 0.68–0.83 (m, 18H). ^{31}P {^{1}H} NMR (DMSO-d_6, room temperature, 121.4 MHz) δ (ppm): 10.01 ppm (s, ^{195}Pt satellites, $^1J_{Pt-P}$ = 2,638.9 Hz). ESI-TOF-MS: *m/z* 836.85 $[M - 6OTf]^{6+}$, 846.53 $[M - 2HNO_3 - 4NO_3 + Na + K]^{6+}$, 1,004.03 $[M - HNO_3 - 5NO_3]^{5+}$, 1,011.42 $[M - 2HNO_3 - 4NO_3 + K]^{5+}$, 1,016.43 $[M - 5NO_3]^{5+}$, 1,254.53 $[M - 2HNO_3 - 4NO_3]^{4+}$, 1,263.53 $[M - 3HNO_3 - 3NO_3 + K]^{4+}$, 1,270.54 $[M - 4HNO_3 - 2NO_3 + Na + K]^{4+}$.

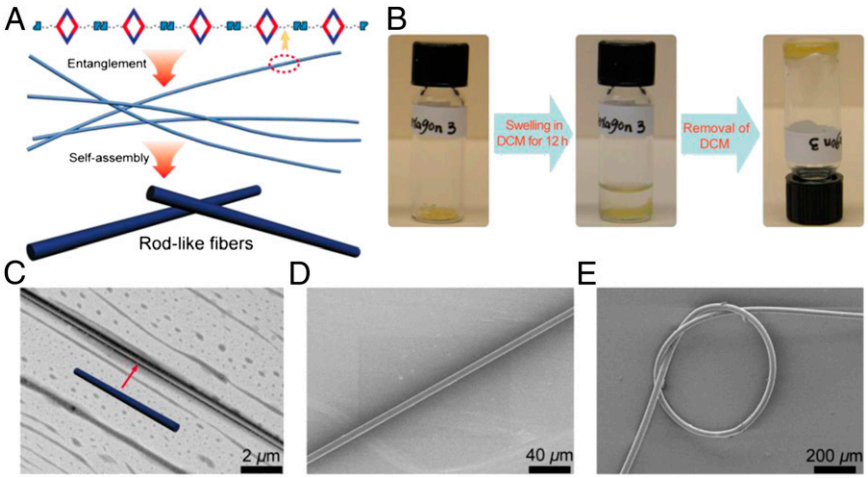

Fig. 5. Solid-state analyses of supramolecular polyrhomboid and hexagonal networks. (*A*) Cartoon representation of the formation of rod-like fibers from self-assembly of rhomboid **1**. (*B*) Swelling experiment of hexagon **3** in dichloromethane for the preparation of gels. (*C*) TEM image of a rod-like fiber made by placing one drop of dichloromethane solution of rhomboid **1** (1.00 mM) onto a carbon-coated copper grid. SEM images of (*D*) a thin-long fiber drawn from the swelled UPy-functionalized hexagon **2** and (*E*) a knotted fiber made from solvent-swelled UPy-functionalized hexagon **3**.

ACKNOWLEDGMENTS. P.J.S. thanks the National Science Foundation (Grant 1212799) for financial support. F.H. thanks the National Natural Science Foundation of China (Grants 91027006 and 21125417) and the Fundamental Research Funds for the Central Universities (Grants 2012QNA3013) for financial support.

1. Campbell BF, Chance MR, Friedman JM (1987) Linkage of functional and structural heterogeneity in proteins: Dynamic hole burning in carboxymyoglobin. *Science* 238(4825):373–376.
2. Hosono N, et al. (2010) Large-area three-dimensional molecular ordering of a polymer brush by one-step processing. *Science* 330(6005):808–811.
3. Wang Y, et al. (2012) Colloids with valence and specific directional bonding. *Nature* 491(7422):51–55.
4. Hemp ST, Long TE (2012) DNA-inspired hierarchical polymer design: Electrostatics and hydrogen bonding in concert. *Macromol Biosci* 12(1):29–39.
5. Hartgerink JD, Beniash E, Stupp SI (2001) Self-assembly and mineralization of peptide-amphiphile nanofibers. *Science* 294(5547):1684–1688.
6. Gan Q, et al. (2011) Helix-rod host-guest complexes with shuttling rates much faster than disassembly. *Science* 331(6021):1172–1175.
7. Yan X, Wang F, Zheng B, Huang F (2012) Stimuli-responsive supramolecular polymeric materials. *Chem Soc Rev* 41(18):6042–6065.
8. Fouquey C, Lehn JM, Levelut AM (1990) Molecular recognition directed self-assembly of supramolecular liquid crystalline polymers from complementary chiral components. *Adv Mater* 2(5):254–257.
9. De Greef TFA, et al. (2009) Supramolecular polymerization. *Chem Rev* 109(11): 5687–5754.
10. Sijbesma RP, et al. (1997) Reversible polymers formed from self-complementary monomers using quadruple hydrogen bonding. *Science* 278(5343):1601–1604.
11. Park T, Zimmerman SC (2006) Formation of a miscible supramolecular polymer blend through self-assembly mediated by a quadruply hydrogen-bonded heterocomplex. *J Am Chem Soc* 128(35):11582–11590.
12. Niu Z, Gibson HW (2009) Polycatenanes. *Chem Rev* 109(11):6024–6046.
13. Liu Y, Yu Y, Gao J, Wang Z, Zhang X (2010) Water-soluble supramolecular polymerization driven by multiple host-stabilized charge-transfer interactions. *Angew Chem Int Ed Engl* 49(37):6576–6579.
14. Wang F, et al. (2010) Metal coordination mediated reversible conversion between linear and cross-linked supramolecular polymers. *Angew Chem Int Ed Engl* 49(6):1090–1094.
15. Niu Z, Huang F, Gibson HW (2011) Supramolecular AA-BB-type linear polymers with relatively high molecular weights via the self-assembly of bis(*m*-phenylene)-32-crown-10 cryptands and a bisparaquat derivative. *J Am Chem Soc* 133(9):2836–2839.
16. Gröger G, et al. (2011) Switchable supramolecular polymers from the self-assembly of a small monomer with two orthogonal binding interactions. *J Am Chem Soc* 133(23): 8961–8971.
17. Folmer BJB, Sijbesma RP, Verseegen RM, van der Rijt JAJ, Meijer EW (2000) Supramolecular polymer materials: Chain extension of telechelic polymers using a reactive hydrogen-bonding synthon. *Adv Mater* 12(12):874–878.
18. Burnworth M, et al. (2011) Optically healable supramolecular polymers. *Nature* 472(7343):334–337.
19. Yan X, et al. (2012) A multiple-responsive, shape-persistent, and elastic supramolecular polymer network gel constructed by orthogonal self-assembly. *Adv Mater* 24(3): 362–369.
20. Aida T, Meijer EW, Stupp SI (2012) Functional supramolecular polymers. *Science* 335(6070):813–817.
21. Fujita M, Tominaga M, Hori A, Therrien B (2005) Coordination assemblies from a Pd(II)-cornered square complex. *Acc Chem Res* 38(4):369–378.
22. Northrop BH, Zheng YR, Chi KW, Stang PJ (2009) Self-organization in coordination-driven self-assembly. *Acc Chem Res* 42(10):1554–1563.
23. De S, Mahata K, Schmittel M (2010) Metal-coordination-driven dynamic heteroleptic architectures. *Chem Soc Rev* 39(5):1555–1575.
24. Adarsh NN, Dastidar P (2012) Coordination polymers: What has been achieved in going from *innocent* 4,4′-bipyridine to bis-pyridyl ligands having a *non-innocent* backbone? *Chem Soc Rev* 41(8):3039–3060.
25. Kreno LE, et al. (2012) Metal-organic framework materials as chemical sensors. *Chem Rev* 112(2):1105–1125.
26. Cook TR, Zheng YR, Stang PJ (2013) Metal-organic frameworks and self-assembled supramolecular coordination complexes: Comparing and contrasting the design, synthesis, and functionality of metal-organic materials. *Chem Rev* 113(1):734–777.
27. Chakrabarty R, Mukherjee PS, Stang PJ (2011) Supramolecular coordination: Self-assembly of finite two- and three-dimensional ensembles. *Chem Rev* 111(11): 6810–6918.
28. Sun QF, Sato S, Fujita M (2012) An $M_{18}L_{24}$ stellated cuboctahedron through post-stellation of an $M_{12}L_{24}$ core. *Nat Chem* 4(4):330–333.
29. Smulders MM, Riddell IA, Browne C, Nitschke JR (2013) Building on architectural principles for three-dimensional metallosupramolecular construction. *Chem Soc Rev* 42(4):1728–1754.
30. Gianneschi NC, Masar MS, 3rd, Mirkin CA (2005) Development of a coordination chemistry-based approach for functional supramolecular structures. *Acc Chem Res* 38(11):825–837.
31. Oliveri CG, Ulmann PA, Wiester MJ, Mirkin CA (2008) Heteroligated supramolecular coordination complexes formed via the halide-induced ligand rearrangement reaction. *Acc Chem Res* 41(12):1618–1629.
32. Yang HB, et al. (2007) A highly efficient approach to the self-assembly of hexagonal cavity-cored tris[2]pseudorotaxanes from several components via multiple noncovalent interactions. *J Am Chem Soc* 129(46):14187–14189.
33. Forgan RS, Sauvage JP, Stoddart JF (2011) Chemical topology: Complex molecular knots, links, and entanglements. *Chem Rev* 111(9):5434–5464.
34. Li S, et al. (2013) Formation of [3]catenanes from 10 precursors via multicomponent coordination-driven self-assembly of metallarectangles. *J Am Chem Soc* 135(6): 2084–2087.
35. Lee SJ, Hupp JT (2006) Porphyrin-containing molecular squares: Design and applications. *Coord Chem Rev* 250(13):1710–1723.
36. Pluth MD, Bergman RG, Raymond KN (2009) Proton-mediated chemistry and catalysis in a self-assembled supramolecular host. *Acc Chem Res* 42(10):1650–1659.
37. Kelley RF, et al. (2008) Intramolecular energy transfer within butadiyne-linked chlorophyll and porphyrin dimer-faced, self-assembled prisms. *J Am Chem Soc* 130(13):4277–4284.
38. Sumida K, et al. (2012) Carbon dioxide capture in metal-organic frameworks. *Chem Rev* 112(2):724–781.
39. Beijer FH, Sijbesma RP, Kooijman H, Spek AL, Meijer EW (1998) Strong dimerization of ureidopyrimidones via quadruple hydrogen bonding. *J Am Chem Soc* 120(27):6761–6769.
40. Kushner AM, Vossler JD, Williams GA, Guan Z (2009) A biomimetic modular polymer with tough and adaptive properties. *J Am Chem Soc* 131(25):8766–8768.
41. Rief M, Gautel M, Oesterhelt F, Fernandez JM, Gaub HE (1997) Reversible unfolding of individual titin immunoglobulin domains by AFM. *Science* 276(5315):1109–1112.
42. Yang HB, Ghosh K, Arif AM, Stang PJ (2006) The synthesis of new 60 ° organometallic subunits and self-assembly of three-dimensional M_3L_2 trigonal-bipyramidal cages. *J Org Chem* 71(25):9464–9469.
43. Li SL, Xiao T, Wu Y, Jiang J, Wang L (2011) New linear supramolecular polymers that are driven by the combination of quadruple hydrogen bonding and crown ether-paraquat recognition. *Chem Commun (Camb)* 47(24):6903–6905.
44. Pollock JB, Cook TR, Stang PJ (2012) Photophysical and computational investigations of bis(phosphine) organoplatinum(II) metallacycles. *J Am Chem Soc* 134(25):10607–10620.